16th World Conference on Earthquake, 16WCEE 2017
Santiago Chile, January 9th to 13th 2017
Paper N° 478 (Abstract 478)
Registration Code: S-N1463325223

EFFECTS OF THE VERTICAL COMPONENT OF NEAR-FAULT EARTHQUAKES ON THE NONLINEAR RESPONSE OF R.C. STRUCTURES RETROFITTED BY DIFFERENT BASE-ISOLATION SYSTEMS

F. Mazza[(1)], M. Mazza[(2)], A. Vulcano[(3)]

[(1)] Researcher, Dipartimento di Ingegneria Civile, Università della Calabria, Rende (Cosenza), Italy, fabio.mazza@unical.it
[(2)] Research fellow, Dipartimento di Ingegneria Civile, Università della Calabria, Rende (Cosenza), Italy, mirko.mazza@unical.it
[(3)] Full professor, Dipartimento di Ingegneria Civile, Università della Calabria, Rende (Cosenza), Italy, alfonso.vulcano@unical.it

Abstract

Reinforced concrete (r.c.) framed buildings designed for vertical loads only or in compliance with inadequate seismic classifications and/or code provisions present in many cases a high seismic vulnerability and need retrofitting. To this end, the insertion of a base-isolation system allows a considerable reduction of the horizontal loads transmitted to the superstructure. However, strong near-fault ground motions, which are characterized by long-duration horizontal pulses and high values of the ratio between the peak value of the vertical acceleration (PGA_V) and the analogous value of the horizontal acceleration (PGA_H), can become critical for a base-isolated structure. More specifically, the horizontal deformability of a base-isolated structure may amplify the inelastic response of the superstructure and induce failure of the isolation system. Moreover, high values of the acceleration ratio $\alpha_{PGA}(PGA_V/PGA_H)$ can notably modify the axial load in r.c. columns, while yielding is expected along the span of the beams, especially at the upper storeys; in addition, elastomeric and sliding bearings can undergo tensile loads and uplifts, respectively. To check the effectiveness of different base-isolation systems for retrofitting a r.c. framed structure located in a near-fault area, a numerical investigation is carried out analyzing the nonlinear dynamic response of the fixed-base and isolated structures. For this purpose, a six-storey r.c. framed building primarily designed (as to be a fixed-base one) in compliance with an old Italian seismic code (1996) for a medium-risk zone, is supposed to be retrofitted by insertion of an isolation system at the base for attaining performance levels imposed by the current Italian code (NTC 2008) in a high-risk seismic zone. In detail, elastomeric (HDLRBs) and friction (steel-PTFE sliding bearings, SBs, or friction pendulum bearings, FPBs) bearings are considered. Besides the (fixed-base) primary structure, three cases of base isolation are studied: HDLRBs acting alone (i.e. EBI structure); in-parallel combination of HDLRBs and SBs (i.e. EFBI structure); FPBs acting alone (i.e. FPBI structure). The EBI, EFBI and FPBI structures are designed assuming the same values of the fundamental vibration period and equivalent viscous damping ratio in the horizontal direction. Then, the nonlinear response of the fixed-base structure is compared with those of the differently isolated structures, considering horizontal and vertical components of seven near-fault ground motions available in the Pacific Earthquake Engineering Research Center database. These motions are selected and scaled on the basis of the design hypotheses adopted for the test structure. The dynamic analyses are carried out using a step-by-step procedure based on a two-parameter implicit integration scheme and an initial stress-like iterative procedure. R.c. frame members are idealized by a two-component model, assuming a bilinear moment-curvature law; the effect of the axial load on the ultimate bending moment of columns is taken into account. The response of an elastomeric bearing is simulated by a model with variable stiffness properties in the horizontal and vertical directions, depending on the axial load and lateral deformation; while the response of a friction bearing is described by a nonlinear force-displacement law, with friction variability depending on sliding velocity and axial load.

Keywords: R.c. base-isolated structures, Elastomeric bearings, Friction bearings, Nonlinear dynamic analysis, Near-fault ground motions.

1. Introduction

Base-isolation of a structure allows a considerable reduction of the horizontal seismic loads transmitted to the superstructure [1]. Different isolation strategies or their combination can be used [2]: more precisely, increasing the fundamental vibration period of the structure, to shift it in the range of low spectral accelerations; limiting the maximum force transmitted to the superstructure, depending on the friction coefficient. Therefore, the isolation systems are usually made with elastomeric bearings (e.g. HDLRBs), sometimes coupled in hybrid combination with steel-PTFE sliding bearings (SBs), or frictional pendulum bearings (FPBs). It is worth noting that in the case of an in-parallel combination of HDLRBs and SBs (i.e. EFBI structure) or FPBs acting alone (i.e. FPBI structure), the base-isolated structure, under particular conditions, behaves as a fixed-base structure: i.e., in the horizontal direction, until the friction threshold of the sliding bearings is not exceeded; in the vertical direction, providing the grid of girders placed at the top of the isolation system with a high stiffness and avoiding uplifts of the SBs or FPs. Moreover, in the case of elastomeric bearings acting alone (i.e. EBI structure), the superstructure behaves as isolated or practically fixed-base along the vertical direction depending on the value, respectively very low or very high, of the ratio $\alpha_{K0}(=K_{V0}/K_{H0})$ between the vertical (K_{V0}) and horizontal (K_{H0}) nominal stiffnesses of the isolation system.

A considerable increase of deformability of an isolated structure, in comparison with that of the corresponding fixed-base structure, may lead to an amplification in the structural response under strong near-fault ground motions, which are characterized by long-duration horizontal pulses. In particular, the frequency content of the motion transmitted by the isolators to the superstructure can become critical for the superstructure when the pulse intensity is such that the superstructure undergoes plastic deformations; also, an amplification in the structural response is possible due to the long duration of the pulse [3]. Moreover, near-fault ground motions are also characterized by high values of the ratio α_{PGA} between the peak value of the vertical acceleration (PGA_V) and the analogous value of the horizontal acceleration (PGA_H), which can become critical for a base-isolated structure. More specifically, high values of α_{PGA} can notably modify the axial load in r.c. columns and the ductility demand along the span of the beams [3], while elastomeric and sliding bearings can undergo tensile loads and uplifts [4], respectively.

The above considerations point out the importance of checking the effectiveness of different isolation systems for retrofitting a r.c. framed structure. For this purpose, a numerical investigation is carried out with reference to a six-storey r.c. framed building, which, primarily designed (as to be a fixed-base one) in compliance with an old Italian seismic code (DM96, [5]) for a medium-risk zone, has to be retrofitted by insertion of an isolation system at the base for attaining performance levels imposed by the current Italian code (NTC08, [6]) in a high-risk seismic zone. Besides the (fixed-base) primary structure, three cases of base isolation are studied: HDLRBs acting alone (i.e. EBI structure); in-parallel combination of HDLRBs and SBs (i.e. EFBI structure); FPBs acting alone (i.e. FPBI structure). The nonlinear analysis of the fixed-base and base-isolated structures is carried out considering the horizontal components of seven near-fault ground motions selected in the Pacific Earthquake Engineering Research center database [7] and scaled on the basis of the design hypotheses adopted for the test structure.

2. Design and modelling of the fixed-base original structure

A typical six-storey residential building with r.c. framed structure, whose symmetric plan is shown in Fig. 1, is considered as test structure. Masonry infill walls are considered as nonstructural elements regularly distributed along the perimeter (Fig. 1a) and in elevation. A simulated design of the original framed building is carried out in accordance with the previous Italian code (DM96, [5]), for a medium-risk seismic region (seismic coefficient: C=0.07) and a typical subsoil class (main coefficients: R=ε=β=1). The gravity loads for the r.c. framed structure are represented by a dead load of 4.2 kN/m^2 on the top floor and 5.0 kN/m^2 on the other floors, and a live load of 2.0 kN/m^2 on all the floors; an average weight of about 2.7 kN/m^2 is considered for the masonry infill walls. Concrete cylindrical compressive strength of 25 N/mm^2 and steel reinforcement with yield strength of 375 N/mm^2 are considered. The geometric dimensions of the lateral, interior and central frames are shown in Fig. 1b, where cross section of deep beams and columns (i.e. corner, perimeter and central) are also reported.

The design is carried out to comply with the ultimate limit states. Detailing for local ductility is also imposed to satisfy minimum conditions for the longitudinal bars of the r.c. frame members: for the beams, a tension reinforcement ratio nowhere less than 0.37% is provided and a compression reinforcement not less than half of the tension reinforcement is placed at all sections; for a section of each column a minimum steel geometric ratio of 1% is assumed, supposing that the minimum reinforcement ratio corresponding to one side of the section be about 0.35%. Finally, the fundamental vibration period and effective mass, expressed as percentage of the total mass (m_{tot}=1634 kNs^2/m), along the ground motion direction (i.e. Y direction in Fig. 1a) are T_{1H}=0.665 s and m_{E1}=76%m_{tot}, respectively.

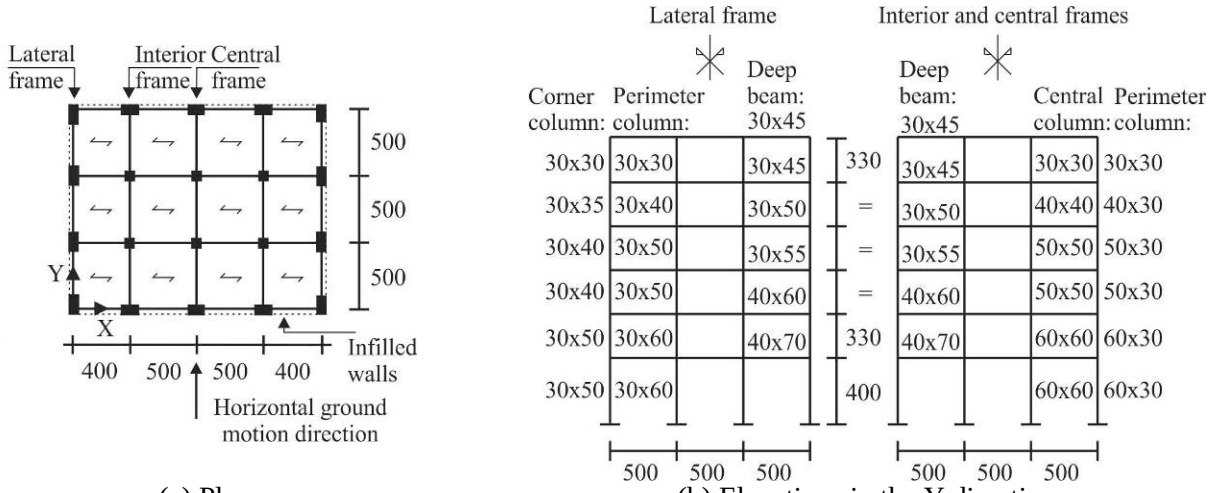

(a) Plan (b) Elevations in the Y direction

Fig. 1 – Fixed-base original structure (units in cm)

The r.c. frame members are idealized by means of a two-component model, constituted of an elastic-plastic component and an elastic component, assuming a bilinear moment-curvature law. The effect of the axial load on the ultimate bending moment of the columns (M-N interaction) is also considered, assuming fully elastic both the axial and shear strains. At each step of the analysis, the elastic-plastic solution is evaluated in terms of the initial state and the incremental load on the basis of a holonomic law, as a solution of the Haar-Kàrmàn principle [8]. More specifically, by imposing plastic conditions on the bending moments (m_i and m_j) at the end sections (i and j) of each frame element, the elastic-plastic solution can be obtained considering, among the equilibrated internal forces $\mathbf{m}=(m_i, m_j)^T$, the one resulting closest to the elastic solution $\mathbf{m}_E=(m_{Ei}, m_{Ej})^T$ and satisfying the complementary energy minimum condition for the self-equilibrated internal forces ($\mathbf{m}$-$\mathbf{m}_E$). The above solution can be easily obtained by using the three-step algorithm illustrated in Fig. 2, where M_{y1} (M_{y4}) and M_{y3} (M_{y2}) represent, respectively, the yield moments producing tension at top and bottom of the end section i (j).

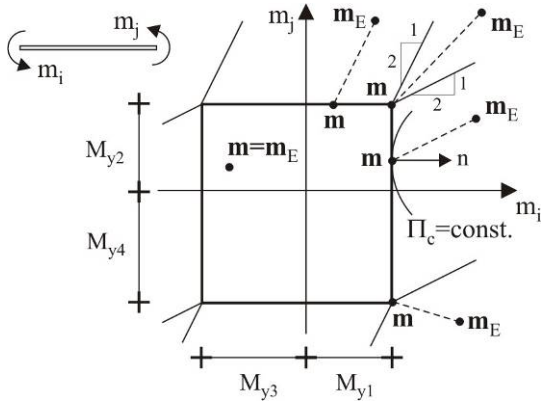

(a)

$$m_i' = \max\left\{-M_{y3}, \min\left\{M_{y1}, m_{Ei}\right\}\right\}$$

$$m_j = \max\left\{-M_{y4}, \min\left\{M_{y2}, m_{Ej} - \frac{1}{2}\left(m_{Ei} - m_i'\right)\right\}\right\}$$

$$m_i = \max\left\{-M_{y3}, \min\left\{M_{y1}, m_{Ei} - \frac{1}{2}\left(m_{Ej} - m_j\right)\right\}\right\}$$

(b)

Fig. 2 – Elastic-plastic solution of r.c. frame member according to the Haar-Kàrmàn principle [8]

For the sake of simplicity, only the horizontal ground motion direction indicated in Fig. 1a is considered for the test structures examined in the numerical investigation. To account for the plastic deformations along the beams induced by the vertical component of the ground motions, each of them is discretized into four sub-elements of the same length. At each step of the analysis, plastic conditions are checked at the potential critical sections of the beams (i.e. end, quarter-span and mid-span sections) and columns (i.e. end sections).

3. Design and modelling of the base-isolated retrofitted structures

To retrofit the six-storey original (fixed-base) framed building, for attaining performance levels imposed by the current Italian code (NTC08, [6]) in a high-risk seismic zone (peak ground acceleration on rock, a_g=0.262g at the life-safety limit state) and medium subsoil class (class C, site amplification factor S=1.319), three in-plan configurations of elastomeric and sliding bearings are considered: (a) EBI structure, with elastomeric bearings acting alone (i.e. high-damping-laminated-rubber bearings, HDLRBs type 1); (b) EFBI structure, with an in-parallel combination of elastomeric (i.e. HDLRBs type 2) and friction (i.e. steel-PTFE sliding bearings, SBs) bearings; (c) FPBI structure, with friction pendulum bearings (i.e. FPBs) acting alone. An additional mass of 511 kNs^2/m, placed above the isolation level, is assumed at the level of the rigid girders, with a cross section of 50x100 cm^2. The base-isolation systems are designed assuming the same values of the fundamental vibration period (i.e. T_{1H}=2.5s) and equivalent viscous damping ratio (i.e. ξ_H=18%). Finally, the (horizontal) design spectral displacement at the NTC08 collapse limit state is assumed equal to 23.33 cm.

3.1 Elastomeric Base-Isolated (EBI) structures

The design of the twenty HDLRBs type 1 of the EBI structure shown in Fig. 3, which are simply assumed with the same dimensions so as to obtain a larger torsional stiffness, is carried out according to the prescriptions imposed by NTC08 at the collapse limit state. Two values of the nominal stiffness ratio of the isolation system, defined as the ratio between the horizontal (K_{H0}) and vertical (K_{V0}) nominal stiffnesses of the HDLRBs, are considered (i.e. α_{K0}=800 and 2000). A shear modulus G=0.4 MPa and a volumetric compression modulus E_b=2000 MPa are assumed for the elastomer.

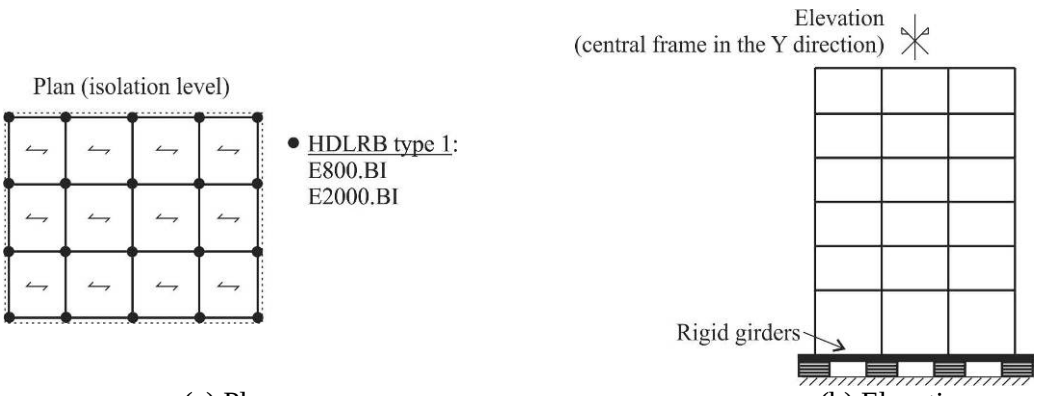

(a) Plan (b) Elevation

Fig. 3 – EBI structures: HDLRBs type 1 acting alone

The HDLRBs fulfill the ultimate limit state verifications regarding the maximum shear strains: i.e. $\gamma_{tot}=\gamma_s+\gamma_c+\gamma_\alpha\leq 5$ and $\gamma_s\leq 2$, where γ_{tot} represents the total design shear strain, while γ_s, γ_c and γ_α represent the shear strains of the elastomer due to seismic displacement, axial compression and angular rotation, respectively. Moreover, the maximum compression axial load (P) does not exceed the critical load (P_{cr}) divided by a safety coefficient equal to 2.0. The maximum allowable tensile stress (σ_{tu}) is assumed as 2G(=0.8 MPa). In Table 1, depending on stiffness ratios α_{K0} considered in the analysis, the base isolation system properties are reported: i.e. the horizontal (K_{H0}) and vertical (K_{V0}) nominal stiffnesses and the corresponding equivalent damping coefficients (C_H and C_V), assuming an equivalent viscous damping ratio in the horizontal direction, ξ_H, equal to

18%, and an analogous ratio in the vertical direction, ξ_V, equal to 5%. The following geometrical and mechanical properties of the HDLRBs are also reported in Table 1: the diameter of the isolator (D); the total thickness of elastomer (t_e); primary (S_1) and secondary (S_2) shape factors; compression modulus (E_c). In Table 1 the results of the verifications for the HDLRBs are also reported. It is interesting to note that the design of the isolators depends on the conditions imposed on the minimum value of P_{cr}/P (i.e. E800.BI) and maximum value of γ_s (i.e. E2000.BI). No tensile forces are found in the isolators.

Table 1 – Properties and results of verifications for HDLRB type 1 acting alone (units in kN, cm and s)

α_{K0}	K_{H0}	K_{V0}	C_H	C_V	D	t_e	S_1	S_2	E_c	γ_s	$\gamma_{tot,max}$	$(P_{cr}/P)_{min}$	$(\sigma_t/\sigma_{tu})_{max}$
800	6.77	5420	0.97	7.59	70.0	22.6	13.24	3.05	32.86	1.03	3.34	2.00	0
2000	6.77	13549	0.97	12.08	53.0	13.3	26.73	4.03	80.00	2.00	4.16	2.56	0

Experimental results [9] pointed out that the horizontal stiffness of a HDLRB (starting from K_{H0}) decreases with increasing vertical load (P), while the corresponding vertical stiffness (starting from K_{V0}) decreases with increasing lateral deformation (u_H). To account for the observed behaviour, the two-spring-two-dashpot model shown in Fig. 4a, constituted of a nonlinear spring acting in parallel with a linear viscous dashpot both in the horizontal and vertical directions, can be adopted [3].

(a) (b)

Fig. 4 – Modelling of the base-isolation system for the EBI structure: HDLRBs acting alone

The nonlinear force-displacement laws for the horizontal (F_K-u_H) and vertical (P-u_V) springs (Fig. 4b) are:

$$F_K = K_H u_H = K_{H0}\left[1-\left(P/P_{cr}\right)^2\right]u_H, \quad P_K = K_V\left(u_V - \frac{\alpha_b}{\alpha_{K0}}\frac{16}{\pi^2 D S_2}u_H^2\right) \tag{1a,b}$$

where the compressive or tensile critical load (P_{cr}) and the vertical stiffness (K_V) can be obtained according to experimental observations [3, 9] and, after some manipulations, can be specialized as

$$P_{cr} = \pm\left(\pi D/4\right)K_{H0}\sqrt{\alpha_{K0}}, \quad K_V = K_{V0}\Big/\left[1+48\left(u_H/\pi D\right)^2\right] \tag{2a,b}$$

where $\alpha_b=h_b/t_r$, h_b and t_r being the total height of the bearing and the total thickness of the rubber, respectively (e.g. $\alpha_b=1.2$ can be considered as a mean value); $S_2=D/t_r$ is the secondary shape factor. Moreover, the linear force-velocity laws for the horizontal (F_C-$\dot{u}_H$) and vertical (P_C-$\dot{u}_V$) dashpots in Fig. 4a are expressed as

$$F_C = C_H\dot{u}_H \cong \left(\xi_H K_{H0} T_{1H}/\pi\right)\dot{u}_H, \quad P_C = C_V\dot{u}_V \cong \left(\xi_V K_{V0} T_{1V}/\pi\right)\dot{u}_V \tag{3a,b}$$

where T_{1H} and T_{1V} represent the fundamental vibration periods in the horizontal and vertical direction, respectively.

3.2 Elastomeric and Friction Base-Isolated (EFBI) structures

The design of the in-parallel combination of HDLRBs type 2 and steel-PTFE SBs for the EFBI structure shown in Fig. 5 is carried out in order to increase the secondary shape factor of the elastomeric bearings (e.g. $S_2 \geq 4$ is a conservative assumption against buckling) in comparison with HDLRBs type 1 shown in Table 1. To this end,

two arrangements of elastomeric and sliding bearings are considered: i.e. four interior SBs (S4), and six interior and two perimeter SBs (S8). Each solution corresponds to a value of the nominal sliding ratio α_{S0}(=$F_{S0}/F_{S0,max}$) of the SBs under gravity loads, defined as the global sliding force (F_{S0}) divided by the maximum sliding force ($F_{S0,max}$); this latter one evaluated supposing that sliding bearings are placed under each column of the test structure. The same nominal stiffness ratios adopted for the EBI structures (i.e. α_{K0}=800 and 2000) are assumed in this case for the HDLRBs type 2.

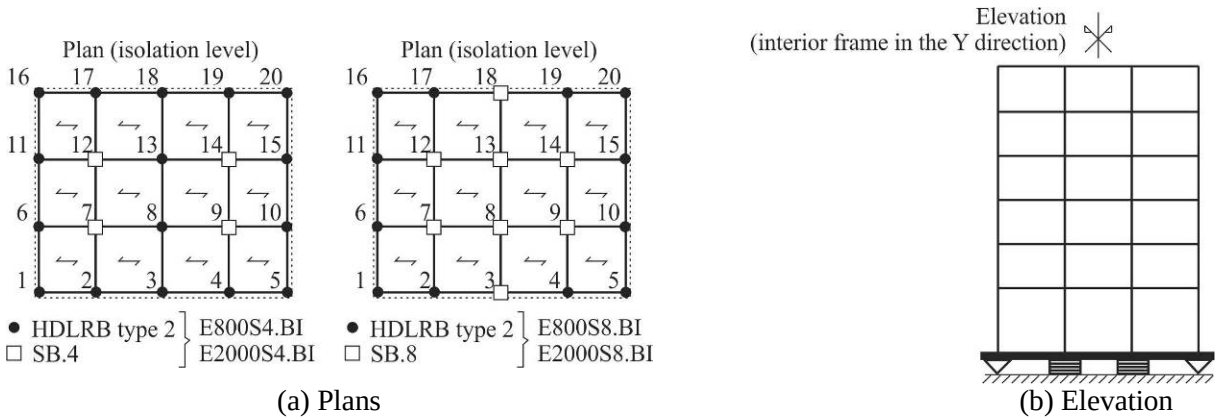

(a) Plans (b) Elevation

Fig. 5 – EFBI structures: in-parallel combination of HDLRBs type 2 and SBs

The equivalent viscous damping in the horizontal direction (ξ_H), for the in-parallel combination of HDLRBs and SBs, is evaluated as

$$\xi_H = \frac{W_{h,HDLRBs} + W_{h,SBs}}{4\pi\left(W_{s,HDLRBs} + W_{s,SBs}\right)} = \xi_{H,HDLRBs} + \xi_{H,SBs} \tag{4}$$

where W_s represents the strain energy

$$W_{s,HDLRBs} = \frac{1}{2}\sum_{i=1}^{n_{HDLRBs}} K_{Hi} \times u_H^2, \quad W_{s,SBs} = \frac{1}{2}\sum_{i=1}^{n_{SBs}} K_{ei} \times u_H^2 = \frac{1}{2}\sum_{i=1}^{n_{SBs}} \mu_{max} \times P_i \times u_H \tag{5a,b}$$

and W_h the hysteretic energy

$$W_{h,HDLRBs} = 4\pi W_{s,HDLRBs} \times \xi_{H,HDLRBs}, \quad W_{h,SBs} = \sum_{i=1}^{n_{SBs}} 4\mu_{max} \times P_i \times u_H \tag{6a,b}$$

being K_{ei} the effective (secant) stiffness of a SB, at the horizontal displacement u_H, and μ_{max} the dynamic-fast coefficient of friction.

The coefficient of friction at sliding velocity $\dot{u}_H$ is evaluated as [10]

$$\mu = \mu_{max} - \left(\mu_{max} - \mu_{min}\right) e^{-\alpha \dot{u}_H} \tag{7}$$

which attains the value μ_{max} or μ_{min} respectively at very high or very low velocity, while α is a constant for given values of pressure and temperature.

Equivalent viscous damping ratios of elastomeric ($\xi_{H,HDLRBs}$) and sliding ($\xi_{H,SBs}$) bearings are calculated in accordance with Eqs. 4-6, referring to the (horizontal) spectral displacement at the collapse limit state (i.e. S_d=23.33cm) and considering the gravity loads and a dynamic-fast sliding friction coefficient μ_{max}=4.2%. Finally, the equivalent viscous damping ratio of the HDLRBs type 2 in the vertical direction is assumed equal to ξ_V=5%. Main properties of the HDLRBs type 2 are reported in Tables 2a and 2b. It is noteworthy that the design of the elastomeric bearings has been limited by the condition imposed on the maximum tensile stress (i.e. $(\sigma_t/\sigma_{tu})_{max}$). Dynamic properties of the SBs are reported in Table 3. The nonlinear dynamic analysis will be carried out assuming μ_{max}/μ_{min}=2.5 and a rate parameter α (see Eq. 7) equal to 5.5 s/m, according to experimental results [11].

The SB response basically depends on sliding velocity, contact pressure and temperature [10, 11]. More specifically, the coefficient of sliding friction increases with increasing velocity up to a certain velocity value, beyond which it remains almost constant, while drops with increasing pressure (with a rate of reduction that is dependent on sliding velocity) and temperature.

The frictional force at the sliding interface of a SB can be expressed as [10]

$$F_f = \mu \times P \times Z \quad (8)$$

where Z is a dimensionless hysteretic quantity (Z takes values of ±1 during sliding and less then unity during sticking).

Table 2a – Properties and results of verifications for HDLRB type 2 with 4 SBs (units in kN, cm and s)

α_{K0}	K_{H0}	K_{V0}	C_H	C_V	D	t_e	S_1	S_2	E_c	γ_s	$\gamma_{tot,max}$	$(P_{cr}/P)_{min}$	$(\sigma_t/\sigma_{tu})_{max}$
800	7.69	6149	0.79	3.43	68.0	19.15	13.70	3.44	34.65	1.22	3.81	2.00	0.6
2000	7.69	15521	0.87	7.91	57.0	13.00	26.73	4.36	80.00	1.80	3.84	3.23	1.0

Table 2b – Properties and results of verifications for HDLRB type 2 with 8 SBs (units in kN, cm and s)

α_{K0}	K_{H0}	K_{V0}	C_H	C_V	D	t_e	S_1	S_2	E_c	γ_s	$\gamma_{tot,max}$	$(P_{cr}/P)_{min}$	$(\sigma_t/\sigma_{tu})_{max}$
800	9.54	7634	0.76	3.16	69.0	15.79	13.02	4.39	32.0	1.48	3.93	2.70	1.0
2000	9.54	19200	0.76	7.64	71.0	16.29	26.73	4.33	80.00	1.43	2.60	5.56	1.0

Table 3 – Properties of the SBs

	α_{K0}	α_{S0}	$\xi_{H,SBs}$	$\xi_{H,HDLRBs}$		α_{K0}	α_{S0}	$\xi_{H,SBs}$	$\xi_{H,HDLRBs}$
S4	800	0.33	4.6%	13.4%	S8	800	0.55	8.4%	9.6%
	2000	0.30	4.2%	13.8%		2000	0.53	8.0%	10.0%

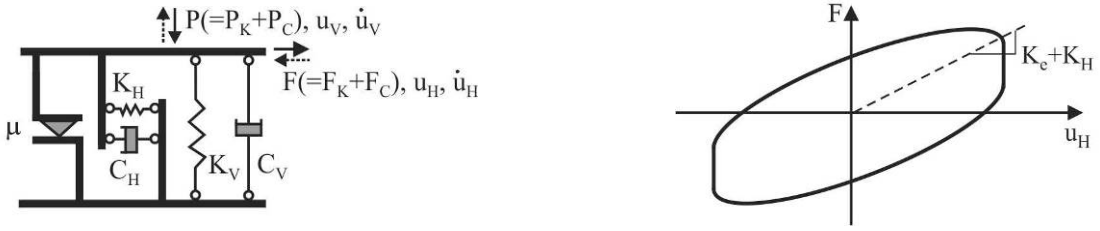

(a) (b)

Fig. 6 – Modelling of the base-isolation system for the EFBI structure: combination of HDLRBs and SBs

3.3 Friction Pendulum Base-Isolated (FPBI) structures

The alternative of using twenty FPBs acting alone, which are simply assumed with the same effective radius of curvature (R) of the sliding interface, is also taken into account in the design of the FPBI structure shown in Fig. 7. More specifically, two in-plan distributions of maximum axial load capacity (P_{Ed}) are assumed for the FP bearings: FP6.BI structure, with six types of FP bearings (having the same μ_{max} value for all isolators); FP2.BI structure, with two types of FP bearings (exhibiting six different μ_{max} values), selected with reference to exterior and interior columns.

For constant values of axial load and friction coefficient, the force-displacement behaviour of the FP bearing in the horizontal direction can be represented by a bilinear law (Fig. 8) with a secant stiffness corresponding to the design displacement ($u_{H,d}$)

$$K_e = P\left(1/R + \mu/u_{H,d}\right) \tag{9}$$

related to effective values of the fundamental vibration period and equivalent viscous damping

$$T_{e,I} = 2\pi\sqrt{\frac{1}{g\left(\frac{1}{R}+\frac{\mu}{u_{H,d}}\right)}};\quad \xi_{e,I} = \frac{2}{\pi}\frac{1}{1+\frac{u_{H,d}}{\mu R}} \tag{10a,b}$$

Moreover, the experimental law derived by a leading world manufacturer of FPBs [12] is assumed, to take into account the law of variability of the dynamic-fast friction coefficient with the quasi-permanent gravity load (P_{sd}) applied on the isolators:

$$\mu_{max} = 2.5\left(P_{sd}/P_{Ed}\right)^{-0.834} \tag{11}$$

with reference to low-type friction characteristic. Main properties of the FPBs of FP6.BI and FP2.BI structures are reported in Table 4. The FP system is designed at the ultimate limit state, requiring the fulfilment of the provisions imposed by NTC08: i.e. maximum compression axial load of the FP bearing (P_{sd}) less than its capacity (P_{Ed}); maximum horizontal displacements less than the spectral value; absence of uplift of the FPs.

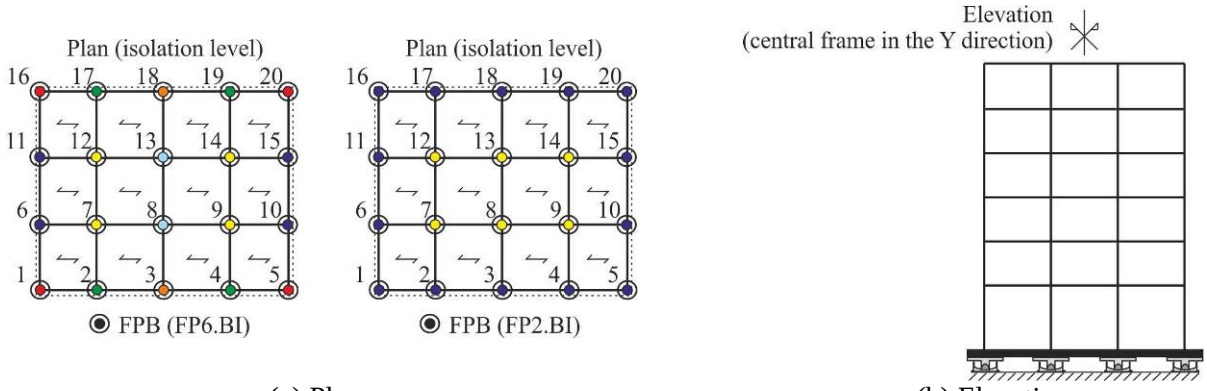

(a) Plans (b) Elevation

Fig. 7 – FPBI structures: FPBs acting alone

(a) (b)

Fig. 8 – Modelling of the base-isolation system for the FPBI structure: FPBs acting alone

Table 4 – Properties of the FPBs (units in kN and cm)

FPB	ξ_H	**R**	P_{sd}	P_{Ed} (FP6.BI)	μ_{max} (FP6.BI)	P_{Ed} (FP2.BI)	μ_{max} (FP2.BI)
1,5,16,20	18%	216	515	970	4.2%	1663	6.7%
2,4,17,19	18%	216	974	1839	4.2%	1663	3.9%
3,18	18%	216	1029	1941	4.2%	1663	3.7%
6,10,11,15	18%	216	1020	1926	4.2%	1663	3.8%

7,9,12,14	18%	216	1458	2753	4.2%	2865	4.4%
8,13	18%	216	1547	2920	4.2%	2865	4.2%

Finally, the nonlinear force-displacement law of a FPB can be represented considering the restoring (F_r) and frictional (F_f) forces shown in Fig. 8

$$F = F_r + F_f = K_r u_H + \text{sign}(\dot{u}_H)\mu P \quad (12)$$

with a lateral restoring stiffness and a fundamental vibration period of the FPB system independent from the mass

$$K_r = P/R; \quad T_I = 2\pi\sqrt{R/g} \quad (13a,b)$$

4. Numerical results

A numerical study is carried out to investigate the main effects produced by the combination of the horizontal and vertical components of near-fault ground motions on the nonlinear response of the (original) fixed-base and (retrofitted) base-isolated structures above described. In the Rayleigh hypothesis, the damping matrix of the superstructure is assumed as a linear combination of the mass and stiffness matrices, assuming a viscous damping ratio in the horizontal ($\xi_{S,H}$) and vertical ($\xi_{S,V}$) direction equal to 2% with reference, respectively, to the two fundamental vibration periods (i.e. $T_{I,H}$ and $T_{I,V}$). Seven near-fault ground motions (EQs) available in the Pacific Earthquake Engineering Research center database [7] are selected, based on the design hypotheses adopted for the test structure (i.e. subsoil class C and high-risk seismic region). For each ground motion attention is focused on the horizontal component showing the largest PGA value together with the vertical component. The main data of the near-fault EQs are shown in Table 5: i.e. earthquake, year, recording station, horizontal component, magnitude (M_w), epicentral distance (Δ), peak ground acceleration in the horizontal (PGA_H) and vertical (PGA_V) directions, peak acceleration ratio α_{PGA}. Moreover, different scale factors (SFs) are considered for the normalization of the near-fault EQs with respect to NTC08 acceleration design spectrum, with reference to the fixed-base and base-isolated structures. More specifically, the selected EQs are normalized with respect to the NTC08 spectrum corresponding to the ultimate life-safety (LS) limit state, considering the Modified Velocity Spectrum Intensity obtained from integration of the velocity (elastic) response spectra in the vertical direction over a defined range of vibration periods [13]. Mean values of the SFs adopted for the selected EQs are reported in Table 6 with reference to FB and isolated structures (see Figs. 3a, 5a and 7a).

Table 5 – Main data of the selected near-fault ground motions

Earthquake	**Recording station**	**M_w**	Δ	**PGA_H**	**PGA_V**	**α_{PGA}**
Imperial Valley, 1979	El Centro D.A.	6.6	5.60 km	0.35 g	0.71 g	2.03
Imperial Valley, 1979	El Centro #7	6.5	3.10 km	0.34 g	0.58 g	1.70
Morgan Hill, 1984	Gilroy #3	6.2	10.3 km	0.19 g	0.40 g	2.04
Coyote Lake, 1979	Gilroy #4	5.7	5.70 km	0.25 g	0.39 g	1.56
Whittier Narrows, 1987	Arcadia	5.9	17.4 km	0.16 g	0.23 g	1.40
Nahanni, 1985	Station I	6.8	6.00 km	0.98 g	2.09 g	2.13
Westmorland, 1981	West. Fire St.	5.6	6.50 km	0.37 g	0.84 g	2.28

Table 6 – Mean scale factors for the selected near-fault ground motions

	FB	**E800.BI**	**E2000.BI**	**E800S4.BI**	**E2000S4.BI**	**E800S8.BI**	**E2000S8.BI**	**FP2.BI**	**FP6.BI**
SF	0.653	0.289	0.351	0.434	0.434	0.653	0.653	0.653	0.653

Firstly, the storey damage at the LS limit state is investigated in Fig. 9 with reference to the maximum values reached, under the selected EQs, by maximum (Fig. 9a) and residual (Fig. 9b) interstorey drift ratios

(=drift/storey height). The drift ratio thresholds related to different damage levels of r.c. elements, in case of nonductile structural systems, are also reported [14]. As shown, the FB structure suffers severe damage with partial collapse due to an irregular vertical distribution of the drift ratio (Fig. 9a). The insertion of elastomeric (e.g. α_{K0}=800) and friction (e.g. α_{S0}=0.30-1.0) base-isolation systems makes the the storey drift distribution almost uniform, reducing the values in the undamaged range for the EBI and EFBI structures and moderately (reparable) damaged range for the FPBI structures. Curves analogous to the previous ones are plotted in Fig. 9b to compare the maximum residual drift ratio obtained for the original (fixed-base) and retrofitted (base-isolated) structures. The residual drift ratio is an important parameter because it represents the irrecoverable part of the interstorey drift, related to damage requiring repair after an earthquake. Note that a highly irregular shape of the residual drift ratio is obtained for the FB structure, while the re-centering properties of HDLRBs and FPBs proves to be very effective for both the EFBI and FPBI structures. Finally, it is interesting to note that maximum effects in terms of storey damage of the base-isolated structures are observed for the highest values of the sliding ratio, which are obtained for the E800S8.BI (i.e. α_{S0}=0.5), FP3.BI and FP6.BI (i.e. α_{S0}=1.0) structures.

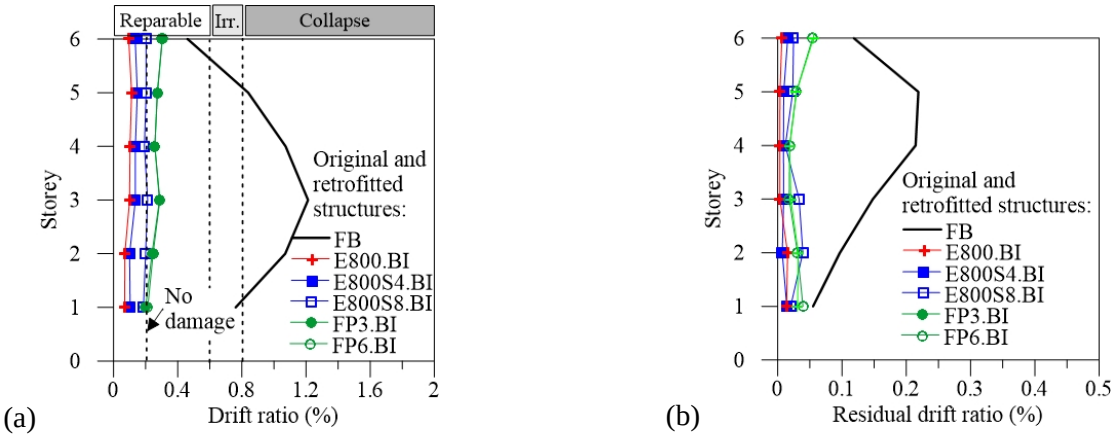

Fig. 9 – Maximum (a) and residual (b) interstorey drift ratio for different elastomeric (α_{K0}=800) and friction (α_{S0}=0.30-1.0) base-isolation systems

Next, to investigate the effects due to the vertical component of the near-fault EQs on r.c. frame members, local structural damage along the building height, in terms of maximum ductility demand of columns (i.e. end sections) and beams (i.e. end, quarter- and mid-span sections), is shown in Figs. 10 and 11. More specifically, the ductility demand is calculated in terms of curvature, assuming as yielding curvature for the columns the one corresponding to the axial load due to the gravity loads. For sake of brevity, only the results for the central frame along the Y direction (see Fig. 1a), having a tributary area for gravity loads greater than those corresponding to the lateral and interior frames, are reported for test structures retrofitted with elastomeric (i.e. α_{K0}=800 in Fig. 10 and α_{K0}=2000 in Fig. 11) and friction (i.e. α_{S0}=0.30-1.0 in Fig. 10 and α_{S0}=0.53-1.0 in Fig. 11) base-isolation systems. As expected, all the base-isolation systems are resulted effective for reducing local damage of r.c. frame members, in comparison with the (original) fixed-base structure. However, unexpected high values of ductility demand are resulted especially at the lower floors, at the end (Figs. 10b and 11b) and quarter-span (Figs. 10c and 11c) sections of beams. This behaviour is more evident for the EFBI and FPBI structures, whose response in the horizontal direction is like that of a fixed-base structure until the friction threshold imposed by the SBs and FPBs, respectively, is not exceeded. Moreover, it is worth noting the limited influence of the α_{K0} value on the ductility demand of the EBI and EFBI structures. On the other hand, the mid-span sections of the beams (Figs. 10d and 11d) undergo increasing ductility demand when assuming an increasing α_{K0} value for the HDLRBs of the EBI and EFBI (especially with four SBs) structures. This behaviour can be explained observing that for rather high values of α_{K0} the superstructure can be considered as a fixed-base structure with reference to the vertical direction. Moreover, a behaviour more similar to that of the original fixed-base structure is obtained in the mid-span sections of the FPBI structures, which are characterized by a sliding ratio α_{S0}=1.0.

Further results, omitted for sake of brevity, highlight that the base-isolation system of the EFBI structures

is characterized by maximum values of γ_s and γ_{tot} greater than those obtained for the EBI structures, but in all the examined cases its failure is not attained under the selected near-fault EQs. Finally, only limited re-centring problems are highlighted for SBs of the E800S8.BI and E2000S8.BI structures and FPBs of FP3.BI and FP6.BI structures, while sufficient restoring capability is obtained for the E800S4.BI and E2000S4.BI structures.

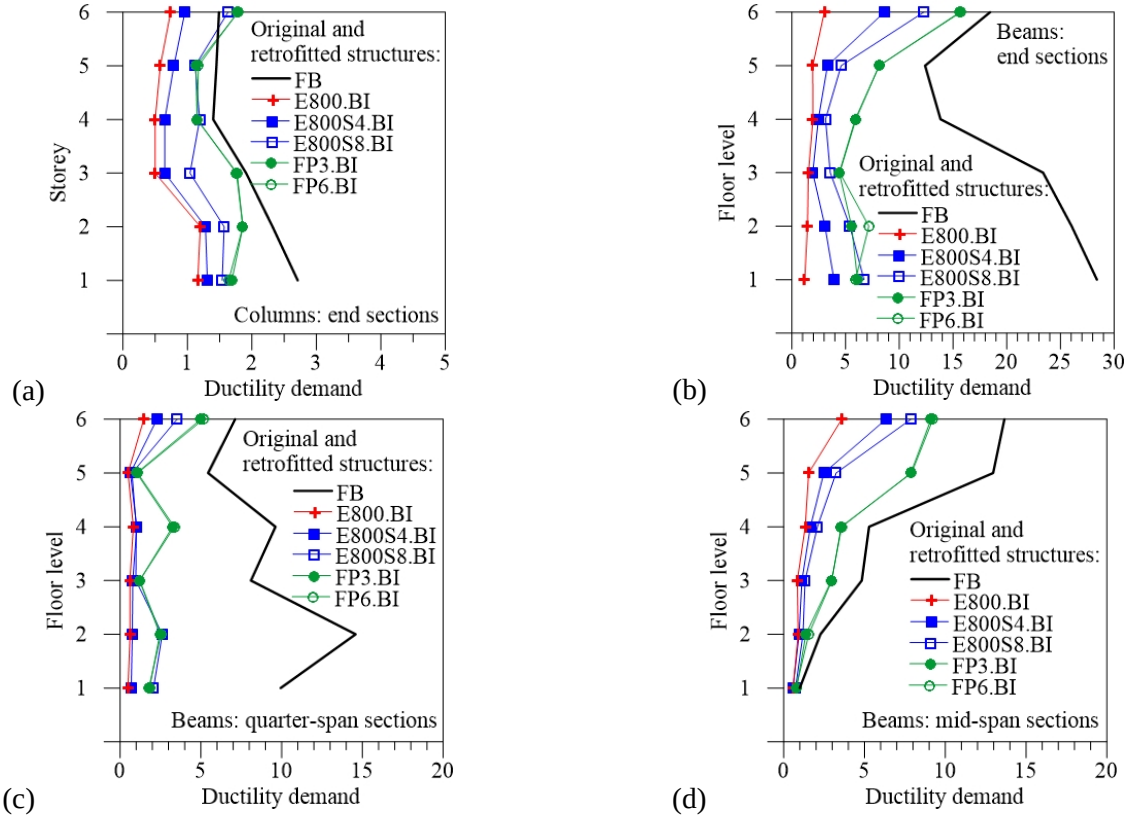

Fig. 10 – Ductility demand for elastomeric (α_{K0}=800) and friction (α_{S0}=0.30-1.0) base-isolation systems

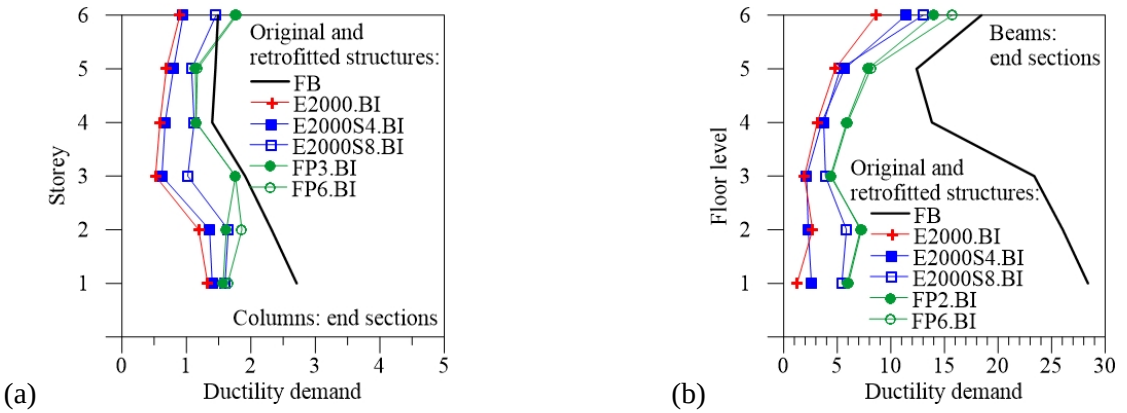

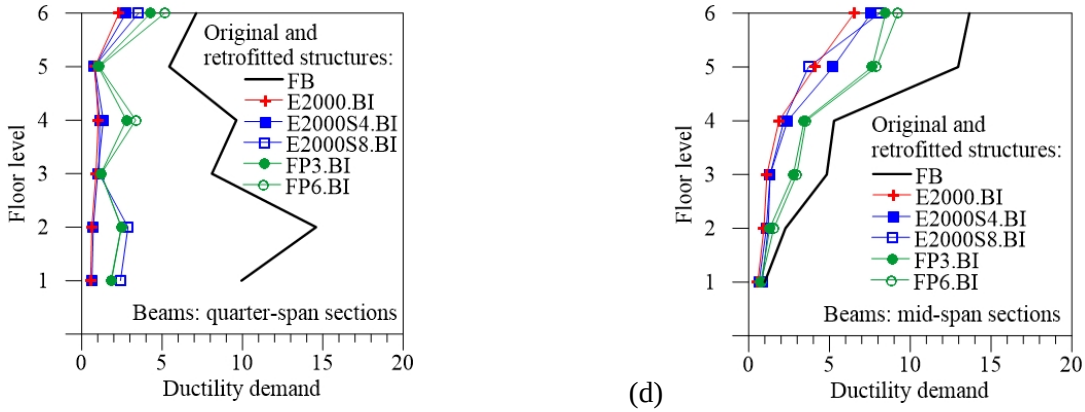

Fig. 11 – Ductility demand for elastomeric (α_{K0}=2000) and friction (α_{S0}=0.53-1.0) base-isolation systems

5. Conclusions

The nonlinear dynamic response of an existing six-storey framed building has been studied under near-fault EQs with high values of the acceleration ratio α_{PGA}. Besides the fixed-base (FB) original structure, three cases of base isolation are compared: HDLRBs acting alone; in-parallel combination of HDLRBs and SBs; FPBs acting alone. Different values of the nominal stiffness ratio α_{K0}, for the HDLRBs, and nominal sliding ratio α_{S0}, for the SBs and FPBs, are also considered. The FB structure suffers severe damage with partial collapse exhibiting an irregular vertical distribution of the maximum drift ratio, but the insertion of elastomeric and friction base-isolation systems makes the storey drift distribution almost uniform, reducing the values in the undamaged (EBI and EFBI structures) and moderately damaged (FPBI structure) ranges. An irregular shape of the residual drift ratio is obtained for the FB structure, while the re-centering properties of HYDBs and FPBs proves to be very effective for the EFBI and FPBI structures. All the base-isolation systems are resulted effective for reducing maximum ductility demand of r.c. frame members, in comparison with the FB structure. Unexpected high values of ductility demand are resulted especially at the lower floors, at the end and quarter-span sections of beams. Moreover, the mid-span sections of the beams undergo increasing ductility demand for an increasing α_{K0} value, when the EBI and EFBI structures are considered. Limited re-centring problems are found for the base-isolation systems with SBs (i.e. E800S8.BI and E2000S8.BI structures) and FPBs (FP3.BI and FP6.BI structures).

6. Acknowledgements

The present work was financed by Re.L.U.I.S. (Italian network of university laboratories of earthquake engineering), in accordance with “Convenzione D.P.C.–Re.L.U.I.S. 2014–16, WPI, Isolation and Dissipation”.

7. References

[1] Naeim F, Kelly JM (1999): Design of seismic isolated structures: from theory to practice. Wiley & S. Ltd, NY.

[2] Mazza F, Mazza M, Vulcano A (2012): Nonlinear dynamic response of rc buildings with different base-isolation systems subjected to horizontal and vertical components of near-fault ground motions. The Open Construction & Building Technology Journal, **6**, 346-354.

[3] Mazza F, Vulcano A (2012): Effects of near-fault ground motions on the nonlinear dynamic response of base-isolated r.c. framed buildings. Earthquake Engineering and Structural Dynamics, **41**, 211-232.

[4] Kasalanati A, Constantinou MC (2005): Testing and modeling of prestressed isolators. Journal of Structural Engineering, **131**, 857-866.

[5] DM96: Italian Ministry of Public Works. Norme tecniche per le costruzioni in zone sismiche e relative istruzioni, D.M. 16-01-1996 and C.M. 10-04-1997, n. 65/AA.GG..

[6] NTC08 (2008): Technical Regulations for the Constructions. Italian Ministry of the Infrastructures (in Italian).

[7] PEER (2008): Pacific Earthquake Engineering Research center. Next Generation Attenuation (NGA) database. http://peer.berkeley.edu/peer_ground_motion_database.

[8] Mazza F, Vulcano A (2010): Nonlinear dynamic response of r.c. framed structures subjected to near-fault ground motions. Bulletin of Earthquake Engineering, **8**, 1331-1350.

[9] Ryan KL, Kelly JK, Chopra AK (2004): Experimental observation of axial load effects in isolation bearings. Procs. of the 13th World Conference on Earthquake Engineering, Vancouver (Canada), paper No. 1707.

[10] Dolce M, Cardone D, Croatto F (2005): Frictional behaviour of steel-PTFE interfaces for seismic isolation. Bulletin of Earthquake Engineering, **3**, 75-99.

[11] Constantinou MC, Mokha A, Reinhorn AM (1990): Teflon bearings in base isolation. II: modeling. Journal of Structural Engineering, **116**(2), 455–474.

[12] FIP Industriale (2013): Catalogue S04. Curved surface sliders, Padova, Italy, http://www.fipindustriale.it.

[13] Mollaioli F, Lucchini A, Cheng Y, Monti G (2013): Intensity measures for the seismic response prediction of base-isolated buildings. Bulletin of Earthquake Engineering, **11**(5), 1841-1866.

[14] Ghobarah A (2004): On drift limits associated with different damage levels. Procs. of the International Workshop Performance-Based Seismic Design: Concepts and Implementation, Bled, Slovenia, 2004.